# Assessment of long-term vicarious calibration efforts of MERIS on land product quality

Schaepman, Michael E ; Zurita-Milla, Raúl ; Kneubühler, Mathias ; Clevers, Jan G P W ; Delwart, Steven

Abstract: Since the launch of MERIS on ENVISAT long term activities using vicarious calibration approaches are set in place to monitor potential drifts in calibration in the radiance products of MERIS. We are using a stable, well monitored reference calibration site (Railroad Valley, Nevada, USA) to derive calibration uncertainties of MERIS over time. We are using interpolation of uncertainties to derive a second set of uncertainties for a national data validation in the Netherlands. A satellite image derived land use map of the Netherlands (LGN4) is used to determine the largest homogeneous land use classes using a standard purity index (SPI). Potential adjacency effects are minimized using moving window filters on the pixels of the aggregated map. Multiple error propagation is being used to assess the impact of calibration accuracy on land use classification. A classification in 9 land use classes is finally performed on MERIS FR images of the Netherlands using image based spectral unmixing and matched filtering with endmembers derived from the LGN. We conclude that the classification performance may significantly be increased, when taking into account long-term vicarious calibration results.

DOI: https://doi.org/10.1117/12.566582

# Assessment of long-term vicarious calibration efforts of MERIS on land product quality

Michael E. Schaepman*[a], Raul Zurita Milla[a], Mathias Kneubuehler[b], Jan Clevers[a], Steven Delwart[c]
[a]Centre for Geo-Information, Wageningen University, The Netherlands;
[b]Remote Sensing Laboratories, University of Zurich, Switzerland;
[c]ESA/ESTEC, Noordwijk, The Netherlands

## ABSTRACT

Since the launch of MERIS on ENVISAT long term activities using vicarious calibration approaches are set in place to monitor potential drifts in calibration in the radiance products of MERIS. We are using a stable, well monitored reference calibration site (Railroad Valley, Nevada, USA) to derive calibration uncertainties of MERIS over time. We are using interpolation of uncertainties to derive a second set of uncertainties for a national data validation in the Netherlands. A satellite image derived land use map of the Netherlands (LGN4) is used to determine the largest homogeneous land use classes using a standard purity index (SPI). Potential adjacency effects are minimized using moving window filters on the pixels of the aggregated map. Multiple error propagation is being used to assess the impact of calibration accuracy on land use classification. A classification in 9 land use classes is finally performed on MERIS FR images of the Netherlands using image based spectral unmixing and matched filtering with endmembers derived from the LGN. We conclude that the classification performance may significantly be increased, when taking into account long-term vicarious calibration results.

**Keywords**: imaging spectroscopy, MERIS, vicarious calibration, product validation, error propagation

## 1. INTRODUCTION

The Medium Resolution Imaging Spectrometer (MERIS) [1] is one of totally ten instruments on board ESA's ENVISAT platform [2, 3]. MERIS is a 68.5° field-of-view pushbroom imaging spectrometer that measures the solar radiation reflected by the Earth, at a ground spatial resolution of 300 m in full resolution (FR) and 1200 m at reduced resolution (RR), and in totally 15 spectral bands covering the visible and near infra-red region of the electromagnetic spectrum. MERIS allows global coverage of the Earth in 3 days. MERIS data products provided by ESA include georeferenced TOA radiance data (Level 1b) as well as various water [4], land [5, 6] and atmospheric products [7, 8] (Level 2), as well analytical tools for end users to access the data [9, 10]. The radiometric data quality of MERIS [11] is based on several calibration efforts, including on-board diffuser calibration [12, 13] and vicarious calibration [14, 15, 16], amongst others. We are using in this paper the latest calibration results that include the treatment of all the above efforts to demonstrate the impact on the calibration accuracy and finally on the product side on the land use mapping quality.

## 2. METHODS AND DATA CALIBRATION

### 2.1 VICARIOUS CALIBRATION

In the context of this paper, we consider vicarious calibration to include all relevant calibration steps that are required to convert raw sensor data into accurate and useful radiometric quantities that are simultaneously measured on ground and at sensor. Vicarious calibration is therefore an independent method for monitoring instrument radiometric performance, including error assessment with reflectance standards, field instruments and atmospheric radiation measurements. This particular experiment follows a so called reflectance-based approach with ground measurements of the atmospheric optical depth and surface reflectance over a bright natural target We are subsequently extrapolating the such achieved

* Michael.Schaepman@wur.nl; phone +31 317 47 46 45; fax +31 317 47 90 00; http://www.dow.wur.nl/UK/cgi/

Sensors, Systems, and Next-Generation Satellites VIII, edited by Roland Meynart, Steven P. Neeck, Haruhisa Shimoda, Proceedings of SPIE Vol. 5570 (SPIE, Bellingham, WA, 2004) · 0277-786X/04/$15 doi: 10.1117/12.566582

calibration uncertainties at top of the atmosphere (TOA) to acquisition orbits located in-between two given vicarious calibration attempts, by assuming that the radiometric uncertainty remains stable (e.g., linearly interpolate able) between these acquisitions. This approach follows in certain ways the so called QUASAR [17, 18] approach, but does not support simultaneous airborne instrument acquisitions.

### 2.1.1 Railroad Valley Playa Test Site

The dry lakebed of Railroad Valley Playa (RRVP), Nevada, USA is located at 1.35 km above sea level (38.504° N latitude, 115.692° W longitude). It is a desert site with no vegetation. Temporal records for this site show reflectance variations as a function of time of year, with lowest reflectance in the winter months due to a rising water table. The accuracy of vicarious calibration experiments over land is highly dependent on the choice of an appropriate calibration target. Ideally, such a calibration site should be flat, bright, spatially uniform, and spectrally stable over time, near lambertian for small angles off nadir, and of sufficiently large spatial extent. Desert playas are preferred for vicarious calibration of moderate spatial resolution sensors due to their optical properties, predictably sunny conditions and low atmospheric aerosol loading. In this experiment, in-situ sunphotometer data from all dates of MERIS acquisitions were available. MODTRAN-4 [**19, 20**], a radiative transfer code (RTC) is used, constrained by field data, to calculate the top-of-atmosphere radiance present at the sensor. Input parameters include ground measurements of the surface reflectance, sun-target-sensor geometries and atmospheric properties (aerosol model, horizontal visibility). The method is described in detail in [**14**].

Figure 1 lists in detail the achieved vicarious calibration uncertainty for each spectral band of MERIS. The bands affected most by the atmosphere (e.g., 11 and 15) have been rescaled due to larger uncertainties in these graphs.

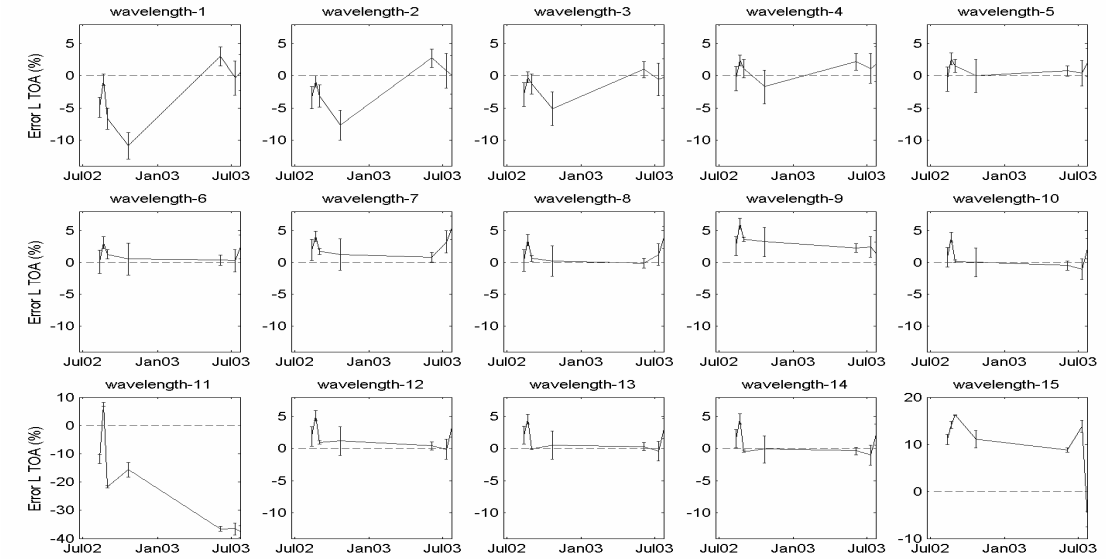


Figure 1: Temporal evolution of calibration uncertainty for vicarious calibration in all 15 MERIS spectral bands between July 2002 and July 2003. RMS errors are plotted on the y-axis, and band 11 and 15 have different y-axis scaling than the other bands.

## 2.2 MERIS DATA AVAILABILITY AND PROCESSING

For this particular experiment, programming requests were scheduled to acquire MERIS FR (Full Resolution) 1b data over RRVP and the Netherlands. Figure 2 lists all the MERIS acquisitions that have been made. Out of 32 full coverage's of the Netherlands between July 2002 and April 2004 (top line), 11 were considered to be cloud free (second line from top, less than 1/8 cloud cover) and three scenes have finally been selected as reference (bottom line). The further reduction by 8 scenes is a result of partial cloud cover over the most important ground reference sites in the

Netherlands. In the same period 7 acquisitions in RRVP have been taken place (second line from bottom), such that sufficient scenes were available to propagate uncertainties in a linear way.

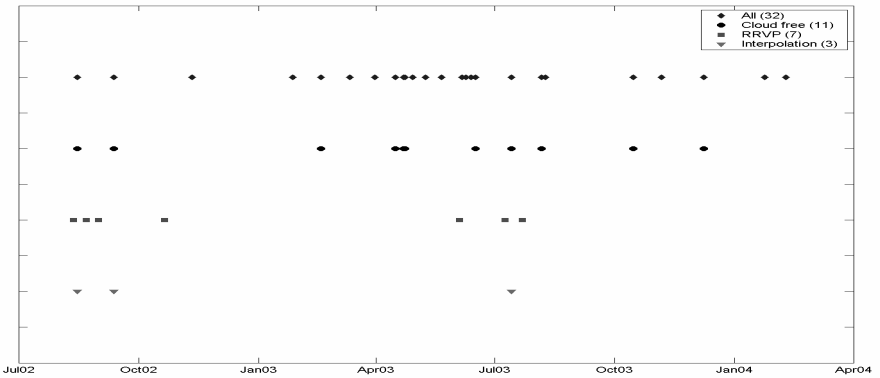


Figure 2: MERIS FR Level 1b acquisitions over the Netherlands (top two and bottom line), as well as Railroad Valley Playa (second line from bottom). 7 RRVP and 3 Netherlands scenes were finally selected for further processing.

Using the RRVP data, the relative mean error (RME) was calculated for all the spectral bands of MERIS, assuming that there is a linear evolution of the vicarious calibration derived uncertainty. Subsequently these uncertainties were first interpolated between RRVP acquisitions and Netherlands acquisitions and then the RME was computed using the following equation (eq. 1):

$$RME = 100 \cdot \left( \frac{R_{MERIS\_TOA} - R_{VC\_TOA}}{R_{MERIS\_TOA}} \right) \qquad (1)$$

where $R_{MERIS\_VC}$ is the corrected ('true') value and $R_{MERIS\_TOA}$ is the actually measured value. Following eq. 1, the correction factors for calibration differences can be computed following eq. 2:

$$R_{VC\_TOA} = R_{MERIS\_TOA} \cdot \left( 1 - \frac{RME}{100} \right) \qquad (2)$$

The application of eq 2. results in band specific correction factors for all three acquisition dates used in the Netherlands (c.f., Table 1).

MERIS data over the Netherlands were reprojected into the Dutch National reference coordinate system (RD) and overlayed with a vector map of coast boundaries to assess the co-registration accuracy of the three acquisition dates. Due to small geometric shifts in-between images, MERIS data was coregistered using ground control points and image-toimage registration to achieve pixel level accuracy.

| Band | 15/08/2002 | 12/09/2002 | 14/07/2003 |
|---|---|---|---|
| 1 | 1.0360 | 1.0762 | 0.9999 |
| 2 | 1.0260 | 1.0420 | 0.9947 |
| 3 | 1.0208 | 1.0216 | 1.0042 |
| 4 | 0.9954 | 0.9951 | 0.9858 |
| 5 | 0.9953 | 0.9882 | 0.9892 |
| 6 | 0.9891 | 0.9884 | 0.9882 |
| 7 | 0.9736 | 0.9831 | 0.9591 |
| 8 | 0.9869 | 0.9942 | 0.9765 |
| 9 | 0.9631 | 0.9643 | 0.9791 |
| 10 | 0.9822 | 0.9981 | 0.9973 |
| 11 | 1.0597 | 1.2024 | 1.3689 |
| 12 | 0.9710 | 0.9900 | 0.9876 |
| 13 | 0.9715 | 0.9989 | 0.9903 |
| 14 | 0.9753 | 1.0035 | 0.9972 |
| 15 | 0.8800 | 0.8499 | 0.9376 |

Table 1: MERIS FR Level 1b correction factors interpolated from RRVP vicarious calibration experiments to acquisitions in the Netherlands.

### 2.3 LAND USE DATABASE

For the Netherlands, the Dutch land use database (LGN) is used as reference. The database uses a grid structure with a cell size of 25 meters; the scale is about 1:50.000. The nomenclature of the LGN4 database contains 39 classes covering urban areas, water, forest, various agricultural crops and ecological classes. LGN is created for an important part on the base of satellite imagery, but also other data sources are integrated into the database. Currently four versions exist ranging from LGN1 to LGN4, spanning a time period between 1986 and 2000. In this study we are using exclusively LGN4, which is based on satellite data of 1999 and 2000. The overall classification accuracy is (depending on class type) between 85-90 % [**21**].

The initial LGN4 is based on 39 land use classes, which were for MERIS aggregated into 9 main land cover classes. These classes are: grassland, arable land, greenhouses, deciduous forest, coniferous forest, water, built-up areas, bare soil (incl. sand dunes), and natural vegetation (c.f., Figure 3, left).

In order to support the selection of pure endmembers, while using LGN4 as a reference, the database was resampled from 25 to 300 m to match the MERIS FR pixel size. The aggregation method is based on using a majority filter with a kernel size of 12 pixels (25 m * 12 = 300m). The land use with the highest abundance in the 12 by 12 kernel was used to label the new land use type. Due to the very heterogeneous land use in the Netherlands, the proportion of every class within the kernel was also recorded during the aggregation process, such that a so called standard purity index (SPI) could be calculated from each window, as noted in eq. 3:

$$SPI = \sqrt{\frac{\sum_{i=1}^{i=n}\left(f_i - f_{\max class}\right)^2}{n-1}} \quad (3)$$

where $f$ represents the fraction of each land use in the kernel, $f_{\max class}$ is the maximum fraction (the class driving the labeling process), and $n$ is the number of classes. Consequently $SPI = 1$, when only one class is present in the kernel window. A threshold of $SPI = 0.9$ was defined as minimum criteria for all the classes except for the greenhouse where SPI was usually around 0.6. This class was then avoided in the further process of defining pure pixels. Once relevant

pixels of a purity of 90% or higher were identified, a moving window filter was applied on the selection of images. This filter is used to minimize adjacency effects and selects only pixels that are surrounded by the same land use class. Figure 3 (right) displays all the pixels that are meeting the homogeneity criteria as developed above. The largest homogeneous class is obviously water, which was not considered in this experiment, whereas grassland is the second largest class.

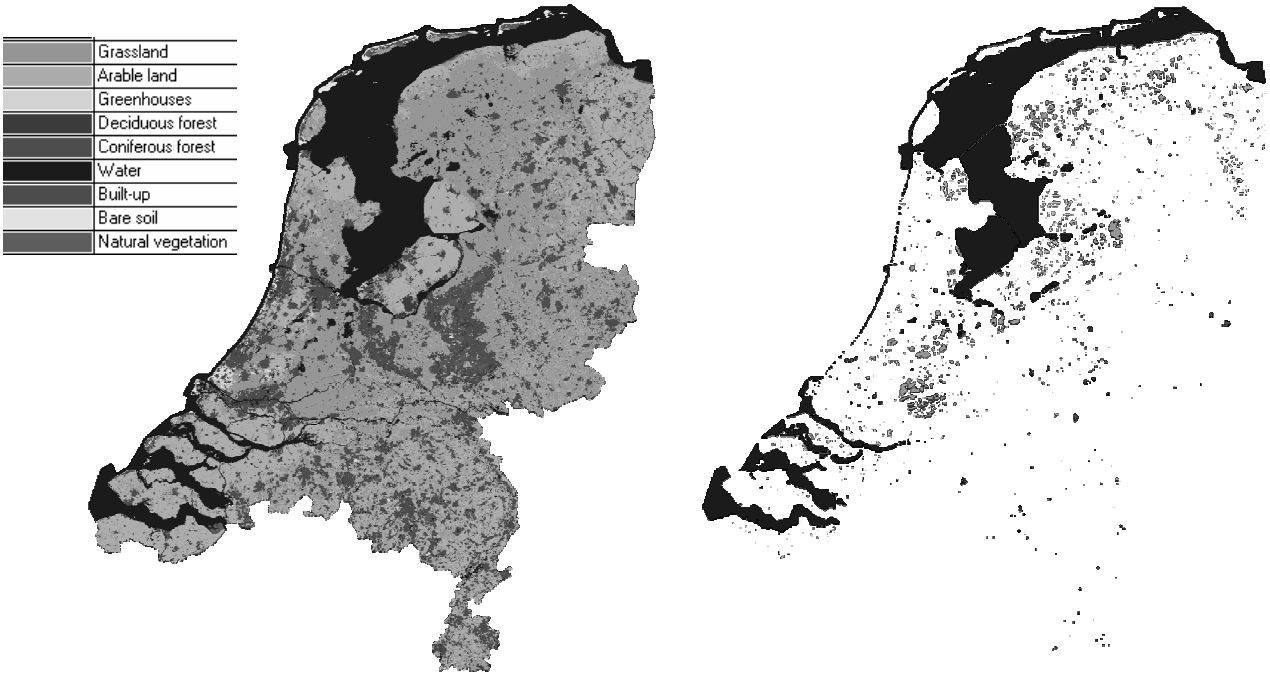


Figure 3: Left: The Dutch land use database LGN4 aggregated into 9 land use classes and resampled to 300 m pixel size. Right: 'Pure' pixel selection in the Netherlands using the Standard Purity Index (SPI).

## 2.4 SPECTRAL UNMIXING

After having identified the proper location of homogenous areas in the Netherlands, for each of the nine classes the spectral signatures can be derived. Figure 4 plots the spectral signatures that have been derived from the MERIS data based on the location identification in LGN4. The corresponding numbers of 300 x 300 m pixels used to derive these endmembers are listed in Table 2.

| Land use | # pixels |
|---|---|
| Greenhouses | 25 |
| Grassland | 4927 |
| Arable land | 2629 |
| Deciduous forest | 33 |
| Coniferous forest | 201 |
| Water | 58285 |
| Built up areas | 390 |
| Bare soil | 132 |
| Natural vegetation | 169 |

Table 2: Number of identified homogenous pixels per aggregated land use class in LGN4.

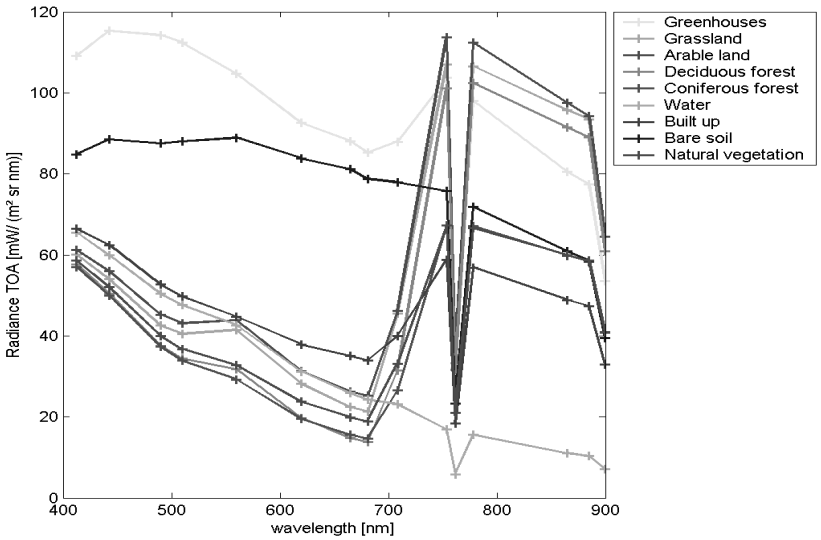


Figure 4: Mean MERIS TOA spectral signatures of nine land use classes as defined in the LGN4 database.

After having identified the most 'pure' endmembers for the nine land use classes, we are using two methods to assess the classification accuracy: Unconstrained linear spectral unmixing [**22, 23**] and matched filtering [**24**] are applied to unmix the time series of three MERIS images. The latter approach turned out to be very useful, since it maximizes the response of a known endmember and suppresses the response of the composite unknown background, thus matching the known signature. It also provides a rapid method of detecting specific classes based on matches to specific library or image endmember spectra.

## 3. RESULTS

Three MERIS images (July 14, August 15, and September 12) in their original form (N) and fully calibrated (VC) form according to Table 1 were available for application of either spectral unmixing or matched filtering. We have performed the endmember selection based on two approaches: either endmembers were selected on the same image as they have been applied to (resulting in the case N_N or VC_VC); or we have selected the endmembers from the corrected image (VC) and applied to the uncorrected image (N, resulting in the case N_VC). For consistency, the opposite analysis was performed as well (VC_N). Due to increased atmospheric attenuation and large uncertainties, MERIS bands 1, 2, 11 and 15 were excluded as well, resulting in 11 spectral bands. The degrees of freedom and the dimensionality analysis nevertheless required not to choose any number below 11 bands.

Table 3 plots the classification accuracy of mapping 9 classes using different approaches and combinations based on the linear spectral unmixing approach. The same approach is used in Table 4, where the results are based on the matched filtering approach.

Table 5 indicates the root mean square errors of unconstrained linear spectral unmixing approach for 15 and 11 spectral bands respectively. The RMSE is listed as mean value plus its standard deviation. The standard deviation is a result of the spatial distribution of the error and Figure 5 plots the spatially distributed RMSE per pixel.

| Date | Image | Endmember | 15 bands | 11 bands |
|---|---|---|---|---|
| 12_sep | N | N | 25.12% | 29.80% |
| 12_sep | N | VC | 16.94% | 8.96% |
| 12_sep | VC | N | 28.81% | 12.47% |
| 12_sep | VC | VC | 24.75% | 29.83% |
| 14_jul | N | N | 25.98% | 28.36% |
| 14_jul | N | VC | 1.67% | 4.79% |
| 14_jul | VC | N | 9.35% | 11.12% |
| 14_jul | VC | VC | 24.99% | 35.37% |
| 15_aug | N | N | 23.36% | 18.73% |
| 15_aug | N | VC | 11.20% | 1.68% |
| 15_aug | VC | N | 15.77% | 10.21% |
| 15_aug | VC | VC | 22.46% | 18.72% |

Table 3: MERIS TOA classification accuracy performed for 9 land use classes based on the linear spectral unmixing approach.

| Date | Image | Endmember | 15 bands | 11 bands |
|---|---|---|---|---|
| 12_sep | N | N | 51.65% | 50.91% |
| 12_sep | N | VC | 28.60% | 38.04% |
| 12_sep | VC | N | 25.66% | 38.15% |
| 12_sep | VC | VC | 51.65% | 50.91% |
| 14_jul | N | N | 57.24% | 57.27% |
| 14_jul | N | VC | 24.36% | 40.86% |
| 14_jul | VC | N | 23.97% | 44.14% |
| 14_jul | VC | VC | 57.24% | 57.27% |
| 15_aug | N | N | 53.40% | 52.90% |
| 15_aug | N | VC | 28.90% | 32.41% |
| 15_aug | VC | N | 25.69% | 36.22% |
| 15_aug | VC | VC | 53.40% | 52.90% |

Table 4: MERIS TOA classification accuracy performed for 9 land use classes based on the matched filtering approach.

| Date | Image | Endmember | RMSE MEAN 15 | SD 15 | RMSE MEAN 11 | SD 11 |
|---|---|---|---|---|---|---|
| 15_aug | N | N | 0.227 | 0.353 | 0.086 | 0.326 |
| 15_aug | N | VC | 1.344 | 0.701 | 0.163 | 0.328 |
| 15_aug | VC | N | 1.336 | 0.651 | 0.135 | 0.327 |
| 15_aug | VC | VC | 0.215 | 0.345 | 0.086 | 0.324 |
| 12_sep | N | N | 0.227 | 0.353 | 0.086 | 0.326 |
| 12_sep | N | VC | 1.344 | 0.701 | 0.163 | 0.328 |
| 12_sep | VC | N | 1.336 | 0.651 | 0.135 | 0.327 |
| 12_sep | VC | VC | 0.215 | 0.345 | 0.086 | 0.324 |
| 14_jul | N | N | 0.192 | 0.182 | 0.088 | 0.106 |
| 14_jul | N | VC | 1.582 | 0.626 | 0.205 | 0.114 |
| 14_jul | VC | N | 1.833 | 0.729 | 0.179 | 0.104 |
| 14_jul | VC | VC | 0.195 | 0.191 | 0.086 | 0.104 |

Table 5: Final RMSE values (mean plus standard deviation) for MERIS land use classification using 11 and 15 bands respectively.

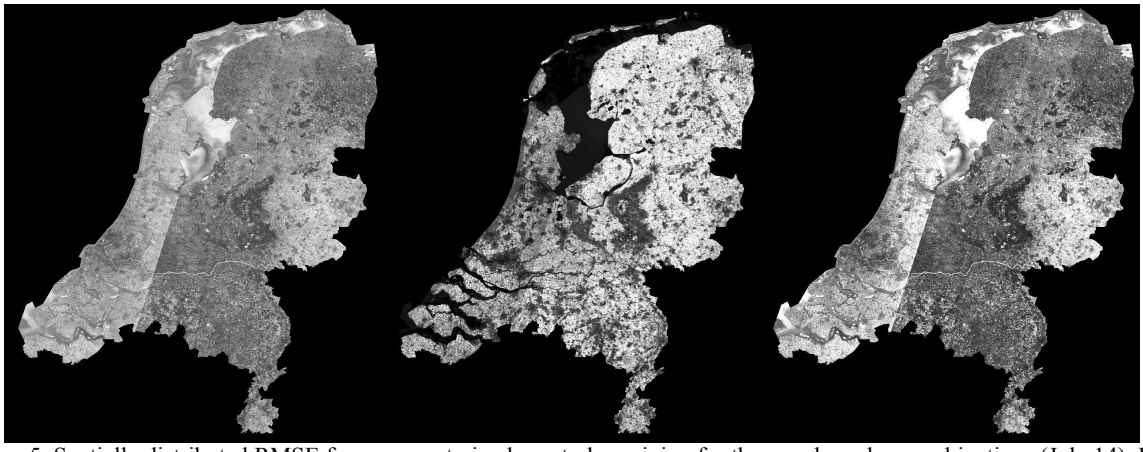

Figure 5: Spatially distributed RMSE from unconstrained spectral unmixing for three endmember combinations (July 14). Left: Image based, uncalibrated (N_N) endmembers; Middle: Calibrated endmembers applied on uncalibrated image (N_VC), and Right: Image based calibrated (VC_VC) endmember selection.

## 4. CONCLUSIONS AND OUTLOOK

We have demonstrated a calibration approach based on MERIS data that can increase the classification accuracy of land use classes significantly. By assuming that non-vicariously calibrated data are being used with well calibrated endmembers in comparison with well calibrated images and endmembers, the classification accuracy could be increased from 23.9% to 57.2% on July 14. Apparently this acquisition date has the best discrimination potential based on the spectral signatures of the 9 land use classes used. Nevertheless also for the other dates, the increase in classification accuracy can be considered as significant, though throughout with lower values.

The overall accuracy of 57% seems to be low in comparison to the achievement of LGN4 (90%), but it must be stated that neither a priori knowledge has been used for this approach, nor ancillary information.

By more closely examining the RMS images in Figure 5, a potential processing artifact is clearly visible in the form of a discrete line reaching from North-West to South-East Netherlands. The MERIS data used for this calibration effort are currently being reprocessed using the latest version of the MERIS processor, which tentatively will remove the artifact. A discontinuity in MERIS camera calibration parameters might be the origin of this line.

The proposed method has been proven to be applicable to discrete land use classification data. Nevertheless, we plan to apply this method by using advanced error propagation methods to estimate the uncertainty of continuous data (eg such as the MERIS Terrestrial Chlorophyll Index (MTCI)), rather than on discrete land use/land cover data.

## ACKNOWLEDGEMENTS

We would like to thank Carsten Brockmann from Brockmann Consult for timely MERIS data processing and delivery. Kurt Thome from the University of Arizona is thanked for providing ground data of the RRVP. The contribution of R. Zurita Milla is granted through the Dutch SRON GO programme (EO-061).

## REFERENCES


1. J.-L. Bézy, S. Delwart and M. Rast, *The esa medium resolution imaging spectrometer meris*, Proceedings of SPIE - The International Society for Optical Engineering 3439 (1998), 594-604.
2. H. Laur, G. Kohlhammer, Y. L. Desnos and S. Coulson, *The envisat mission: Access to the data*, International Geoscience and Remote Sensing Symposium (IGARSS) 1 (2002), 617-619.
3. J. Louet, *The envisat mission and system*, European Space Agency Bulletin (2001), no. 106.
4. D. Antoine and A. Morel, *A multiple scattering algorithm for atmospheric correction of remotely sensed ocean colour (meris instrument): Principle and implementation for atmospheres carrying various aerosols including absorbing ones*, International Journal of Remote Sensing 20 (1999), no. 9, 1875-1916.
5. S. Richard, V. Jéro?me and R. Didier, *Meris level 2 products over land: Validation and potential improvements*, International Geoscience and Remote Sensing Symposium (IGARSS) 3 (2003), 1594-1596.
6. P. J. Curran and C. M. Steele, *Terrestrial meris*, International Geoscience and Remote Sensing Symposium (IGARSS) 6 (2001), 2651-2653.
7. C. Schmechtig, V. Carrère, P. Dubuisson, J. C. Roger and R. Santer, *Sensitivity analysis for the aerosol retrieval over land for meris*, International Journal of Remote Sensing 24 (2003), no. 14, 2921-2944.
8. D. Ramon, R. Santer and J. Vidot, *Meris level 2 products over land: Present status and potential improvements*, Proceedings of SPIE - The International Society for Optical Engineering 4891 (2002), 217-226.
9. G. Levrini and G. Brooker, *Enviview: A gateway to access the envisat data products*, Earth Observation Quarterly (2001), no. 68, 8-11.
10. S. Badessi, H. L. Moeller, P. Viau, D. Castrovillari and B. Collini-Nocker, *The envisat data dissemination system*, European Space Agency Bulletin (2002), no. 109, 12-19.
11. P. Goryl and J. P. Huot, *Overview of the envisat meris and aatsr data quality, calibration and validation program*, International Geoscience and Remote Sensing Symposium (IGARSS) 3 (2003), 1588-1590.
12. G. B. Courrèges-Lacoste, J. G. Schaarsberg, R. Sprik and S. Delwart, *Modeling of spectralon diffusers for radiometric calibration in remote sensing*, Optical Engineering 42 (2003), no. 12, 3600-3607.
13. S. Delwart and L. Bourg, *Meris 1st year: Early calibration results*, International Geoscience and Remote Sensing Symposium (IGARSS) 3 (2003), 1591-1593.
14. M. Kneubuehler, M. E. Schaepman, D. Schläpfer and K. J. Thome, *Meris / envisat vicarious calibration over land*, Proceedings of SPIE - The International Society for Optical Engineering, 2004, p.^pp. 614-623.
15. J. Nieke, M. Hori, T. Aoki, T. Tanikawa, H. Motoyoshi and Y. Nakajima, *Cross-calibration of satellite sensors over snow fields*, Proceedings of SPIE - The International Society for Optical Engineering, 2003, p.^pp. 406-414.
16. Y. M. Govaerts and M. Clerici, *Evaluation of radiative transfer simulations over bright desert calibration sites*, IEEE Transactions on Geoscience and Remote Sensing 42 (2004), no. 1, 176-187.
17. P. M. Teillet, D. N. H. Horler and N. T. O'Neill, *Calibration, validation, and quality assurance in remote sensing: A new paradigm*, Canadian Journal of Remote Sensing 23 (1997), no. 4, 401-414.
18. P. M. Teillet, G. Fedosejevs, R. P. Gauthier, N. T. O'Neill, K. J. Thome, S. F. Biggar, H. Ripley and A. Meygret, *A generalized approach to the vicarious calibration of multiple earth observation sensors using hyperspectral data*, Remote Sensing of Environment 77 (2001), no. 3, 304-327.
19. A. Berk, L. S. Bernstein, G. P. Anderson, P. K. Acharya, D. C. Robertson, J. H. Chetwynd and S. M. Adler-Golden, *Modtran cloud and multiple scattering upgrades with application to aviris*, Remote Sens Environ 65 (1998), no. 3, 367-375.
20. F. X. Kneisys, L. W. Abreu, G. P. Anderson, J. H. Chetwynd, E. P. Shettle, A. Berk, L. S. Bernstein, D. C. Robertson, P. K. Acharya, L. S. Rothman, S. J.E.A., W. O. Gallery and S. A. Clough, "The modtran 2/3 and lowtran 7 model," Ontar Corporation, North Andover, MA, 1995.
21. G. Hazeu, "The dutch land use database lgn," http://www.alterra.wur.nl/UK/cgi/LGN/, 2004.
22. Y. H. Hu, H. B. Lee and F. L. Scarpace, *Optimal linear spectral unmixing*, Ieee Transactions on Geoscience and Remote Sensing 37 (1999), no. 1, 639-644.
23. A. A. Nielsen, *Spectral mixture analysis: Linear and semi-parametric full and iterated partial unmixing in multi- and hyperspectral image data*, International Journal of Computer Vision 42 (2001), no. 1-2, 17-37.
24. J. C. Harsanyi and C. I. Chang, *Hyperspectral image classification and dimensionality reduction - an orthogonal subspace projection approach*, Ieee Transactions on Geoscience and Remote Sensing 32 (1994), no. 4, 779-785.